Chapter 10

Mass Spectrometry of Model Peptides with Shaped Laser Pulses

This chapter describes experimental results obtained with femtosecond pulse shaping as an analytic tool in mass spectrometry of complex polyatomic molecules. As examples the molecules Ac–Phe–NHMe and Ac–Ala–NHMe were studied in this work. They may be considered as model peptides as described in some detail in Sec. 2.2. Both peptides may be seen as prototypes for trying selective bond breaking with shaped strong field pulses in an adaptive feedback loop. Strong field excitation with shaped laser pulses allows one to cleave the strong backbone bonds in the model peptides preferentially, while keeping other, more fragile bonds intact.

10.1 Experimental Results

First, Ac–Phe–NHMe was studied. The molecular beam is produced by evaporation of Ac–Phe–NHMe powder in an oven heated to 395K. Fig. 10.1 presents a typical mass spectrum recorded with laser pulses of $3.7 \times 10^{13}\,\mathrm{W/cm^2}$ peak intensity and $32\,\mathrm{fs}$ pulse duration centred at $797\,\mathrm{nm}$. Rather than the parent ion peak with mass of $220\,\mathrm{u}$, fragments with masses $162\,\mathrm{u}$, $120\,\mathrm{u}$, $87\,\mathrm{u}$, and $43\,\mathrm{u}$ dominate the mass spectrum. A molecular rationalisation of the most relevant fragmentation channels is given in Fig. 10.2.

As one has seen in the previous chapters, mass spectra recorded as a function of laser intensity can provide additional information about photoinduced processes in strong fields. Fig. 10.3 shows the ion signal for the parent ion ($220\,\mathrm{u}$) and its fragments (43 and $162\,\mathrm{u}$) in log-log scale as a function of laser intensity in the range from $2.5 \times 10^{13}\,\mathrm{W/cm^2}$ and

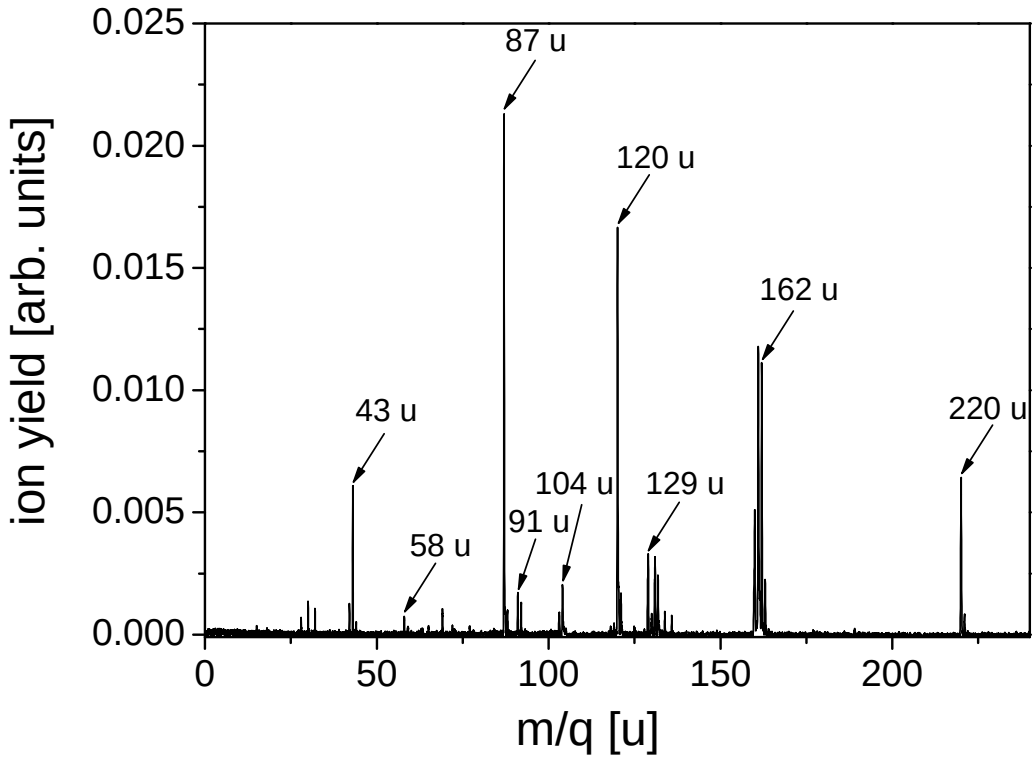

Figure 10.1: Mass spectra of the Ac–Phe–NHMe molecular system recorded with laser pulses of 3.7×10^{13} *W/cm*^{2} *intensity and* 32 *fs pulse duration centred at* 797 *nm.*

1.5×10^{14} W/cm^2 for a laser pulse duration of 34 fs. While a fitting procedure as applied in Chapter 8 to C_{60} would obviously be difficult to perform for these data, the slopes give, nevertheless, evidence of a highly nonlinear behaviour of fragmentation and ionisation of this molecule. Especially, the steeper slope for the 43 u fragment indicates that indeed several photons are needed to ionise the system and cleave this particular bond. All fragment ions tend to saturate eventually as typical for the interaction of strong filed short pulse laser radiation with larger molecules.

To exclude that the observed changes in the fragmentation pattern induced by the optimal pulse is simply an effect of the laser peak intensity, the energy of the unshaped pulse in optimisation experiments was set to the onset of fragmentation at 3.7×10^{13} W/cm^2.

A free optimisation is performed in a first set of experiments. The maximisation of one peptide bond CO–NH (Sec. 2.2) cleavage resulting in a strong enhancement of the CO–CH_3

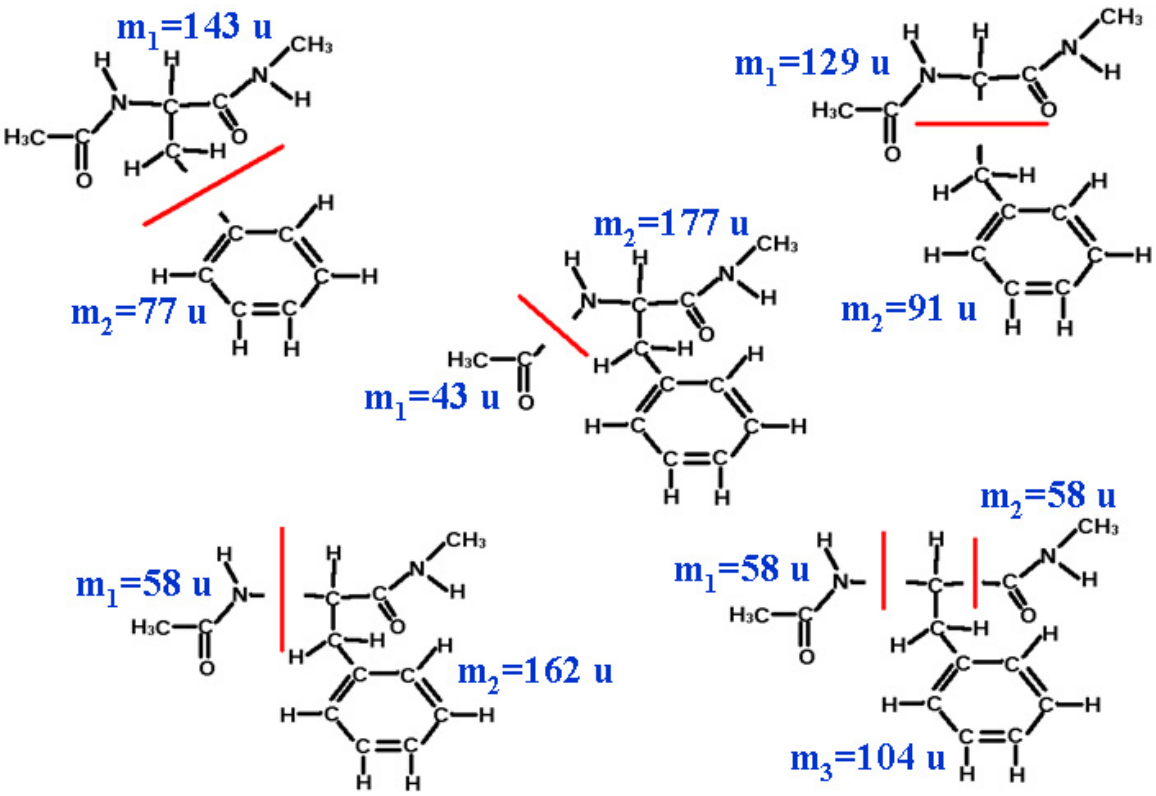

Figure 10.2: Different possible fragmentation channels of the Ac–Phe–NHMe molecular system.

ion (43 u) is chosen as a target for the adaptive control loop, while keeping other bonds intact at will. For that the following fitness criterium

$$f = \left[S(43) - S^0(43)\right] \times \left[S^0(162) - S(162)\right] \tag{10.1}$$

is defined, where $S(43)$ and $S(162)$ are the ion yields of mass 43 u and 162 u, respectively, and the superscript "0" denotes the ion yields obtained with unshaped laser pulses. For individuals returning $S(43) < S^0(43)$ or/and $S(162) > S^0(162)$ the fitness is set to 0 ($f = 0$) and such individuals are excluded from the further evaluation.

A typical learning curve for maximising the CO–NH peptide bond breaking is shown in Fig. 10.4a. The SH-XFROG of the final optimal pulse shape is plotted in Fig. 10.4b. The SH-XFROG map clearly shows that a sequence of $4-5$ pulses with a separation of 156 ± 15 fs is best suited for selective cleavage of this particular peptide bond. Information about the temporal envelope of the laser pulse obtained by projecting the SH-XFROG map onto the time axis is illustrated on the left side of Fig. 10.5. During the optimisation process the signal ration $R = S(43)/S(162)$ increased by a factor of 7.5 compared to the signals recorded with

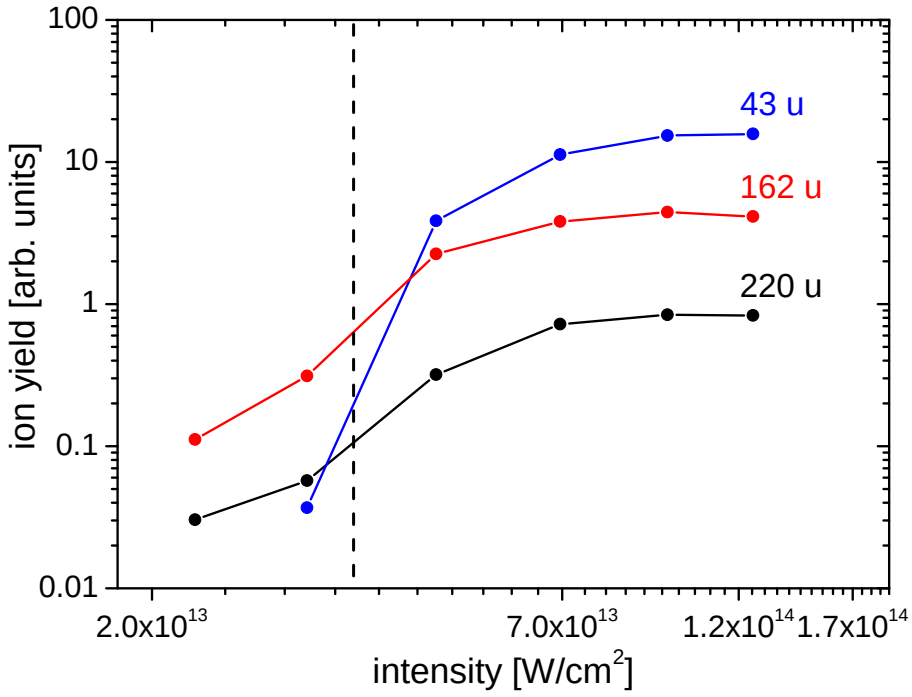

Figure 10.3: Fragment ion yields of mass 43 u, mass 162 u, and the parent ion (mass 220 u) of the Ac–Phe–NHMe molecular system recorded with 34 fs laser pulses plotted as a function of the laser intensity on the log-log scale. The vertical black dashed line indicates the laser intensity utilised in the optimisation experiment.

unshaped pulses (0^{th} generation in Fig. 10.4a) as visible in the corresponding mass spectra on the right side of Fig. 10.5.

For comparison R was measured with a stretched pulse of the same overall duration and energy as the optimal pulse by applying a quadratic spectral phase function to the pulse shaper. The ratio for the optimal pulse is more than 4.5 times larger. Furthermore, in this case the fitness f has a negative value indicating that the signal of both, mass 43 u and mass 162 u increased upon the interaction with elongated pulse. It is known that laser induced fragmentation of large finite systems is mainly determined by the interaction time scale due to efficient energy coupling to nuclear motion, while the excitation pulse is still active as described in Chapter 9. Therefore, the observed general enhancement of fragmentation in model peptides for stretched pulses can be due to efficient heating of nuclear degrees of freedom.

It should be noted that the overall fragmentation pattern with additional major peaks at

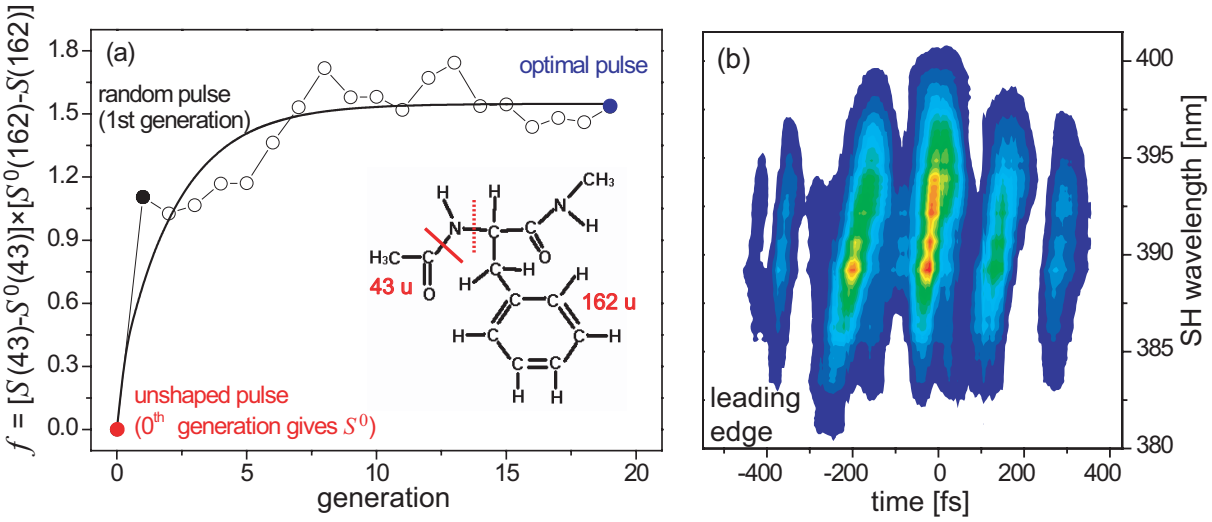

Figure 10.4: (a) Fitness f characterising the predominant formation of fragment mass $43\,u$ as a function of the generation in the adaptive feedback loop. Fluctuations of f are due to experimental noise. The solid line is added to guide the eye. The insert sketches the chemical structure of the Ac–Phe–NHMe molecular system. Both, the optimised bond cleavage resulting fragment mass $43\,u$ and the suppressed one ($162\,u$) are indicated by the straight and dotted lines, respectively. (b) SH-XFROG map of the optimal pulse shape.

mass 87 u and 120 u observed with intense femtosecond pulses – an in particular with the optimally shaped pulse – is quite a bit different from that which has been found in an early single photon photofragmentation study, using UV excitation with 12.1 eV photons utilising a hydrogen discharge tube and a monochromator [OVM74], what is shown for comparison in the upper right panel of Fig. 10.5. The appearance of mass 43 u in the current experiment clearly indicates that strong field effects need to be taken into account to describe the photophysical and photochemical mechanism under fs irradiation.

Due to its stochastic nature each optimisation run leads to a slightly different optimal pulse. Therefore, to see how the optimal results are changed from one optimisation to another 24 individual optimisation runs were performed. The resulting optimal pulse shapes sorted according their shapes of all 24 optimisation experiments is presented in Fig. 10.6. Each column consists of optimal pulses with similar structure and separation between peaks. The colour code indicates values of the fitness f obtained in each optimisation experiment. Often, very similar shapes of optimal pulses result in significantly different values of the fitness f. Hence, not only the temporal pulse structure and therefore intensity is responsible for the observed results, but also the pulse phase and initial conditions of the system as well.

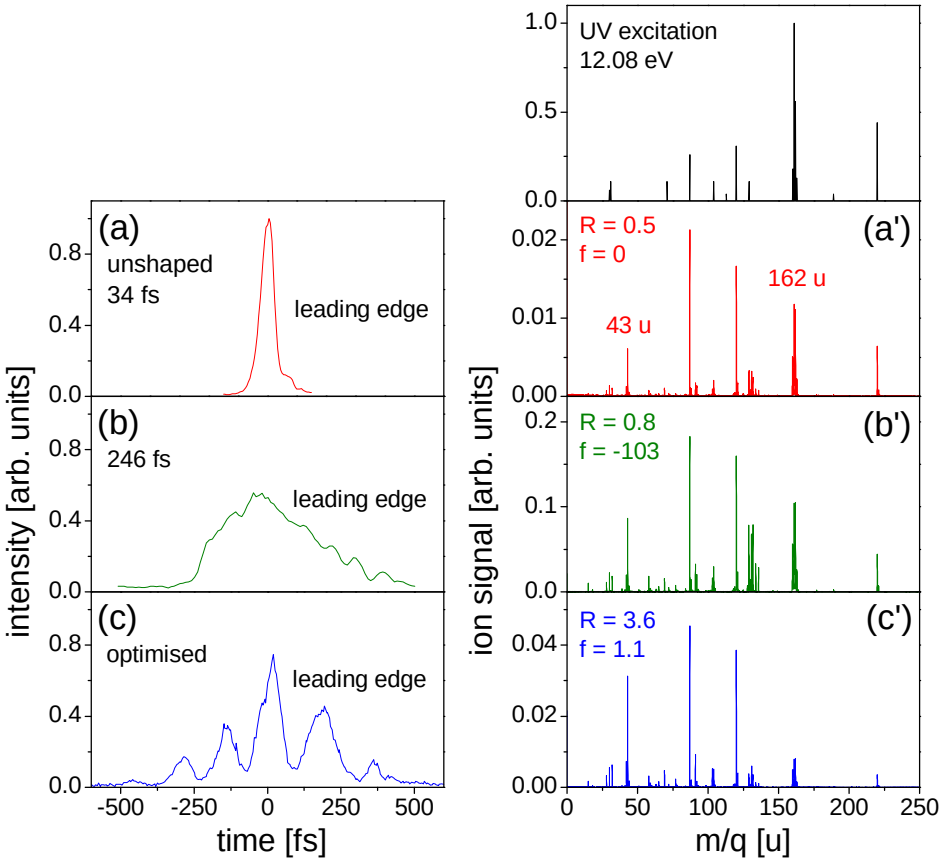

Figure 10.5: Temporal envelope and corresponding mass spectra recorded for the unshaped (a), stretched to 246 fs (FWHM) (b), and optimal pulses (c) are presented. The signal ratios $R = S(43)/S(162)$ and fitness values f are given. For comparison a photofragmentation pattern using a hydrogen discharge tube reconstructed from [OVM74] is plotted in the upper right corner.

To investigate the influence of the pulse phase on the present optimisation in a second set of experiments an optimisation with a restricted, parameterised phase function $\varphi(m)$ was performed. Since results of the free optimisation mainly led to a temporal structure with a periodic pulse sequence (see Fig. 10.6), the phase function was chosen to give essentially an equispaced triple pulse. The following sin function [WPS06] is used

$$\varphi(m) = A \sin(a \cdot m + \Phi) + \pi \quad , \tag{10.2}$$

where m is the pixel index ($0 \leq m \leq 639$) in the shaper which is proportional to the wavelength λ. The bias π in Eq. (10.2) just keeps the phase function within the calibration range $0 - 2\pi$

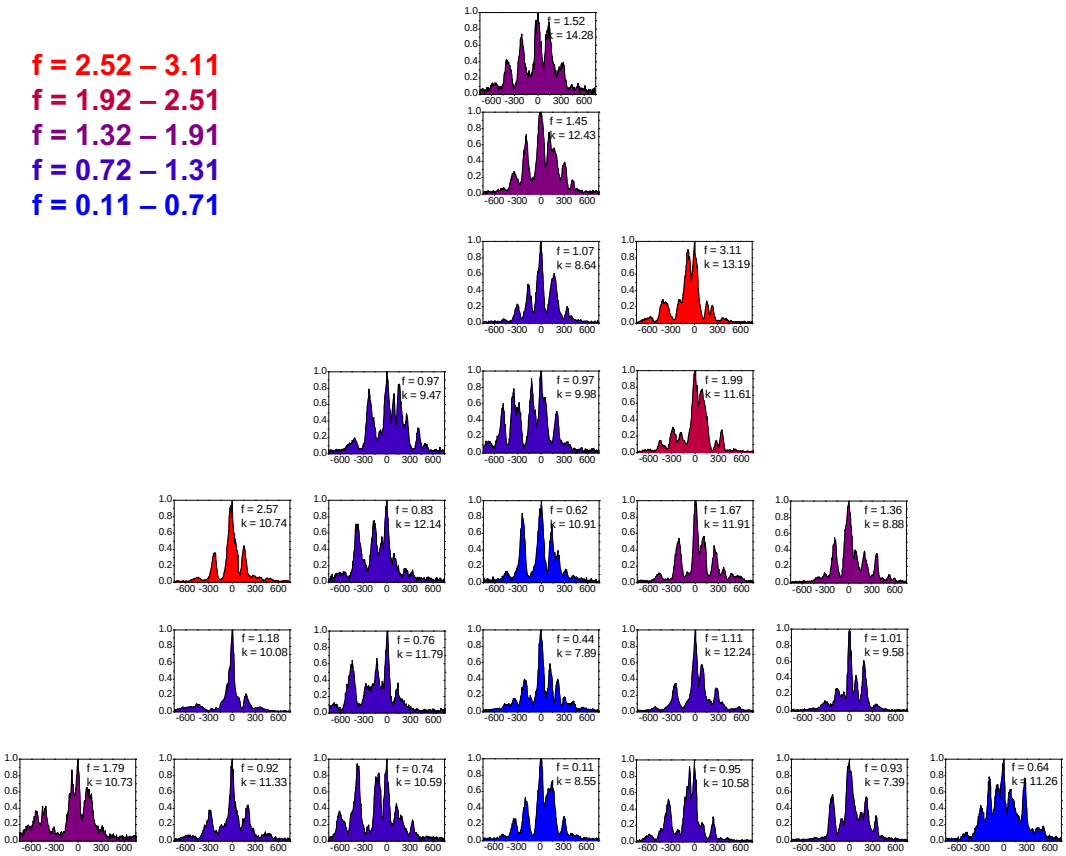

Figure 10.6: Distribution of individual optimal pulses grouped according to the similarities in pulses structure (leading edge on positive delays). Each column consists of optimal pulses with similar structure and separation between peaks. Parameter k is determined as: $k = [S(43)/S(162)] / [S^0(43)/S^0(162)]$. Colour code corresponds to a value of the fitness f.

of the LC array and has no influence on the resulting pulse structure. Due to the small spectral bandwidth across the LC compared to the laser carrier frequency ω Eq. (10.2) can be approximated as

$$\varphi(\omega) \simeq A \sin(\Delta\omega \cdot T + \Phi) + \pi \quad , \tag{10.3}$$

where $\Delta\omega = \omega_0 - \omega_{ref}$ is the difference between the carrier frequency ω_0 and the reference frequency ω_{ref} of the LC calibration, T is the temporal separation between pulses in the pulse sequence (determined experimentally by the parameter a).

Only one free parameter a is used for parameterised optimisation. The parameter $\Phi = \pi/2$

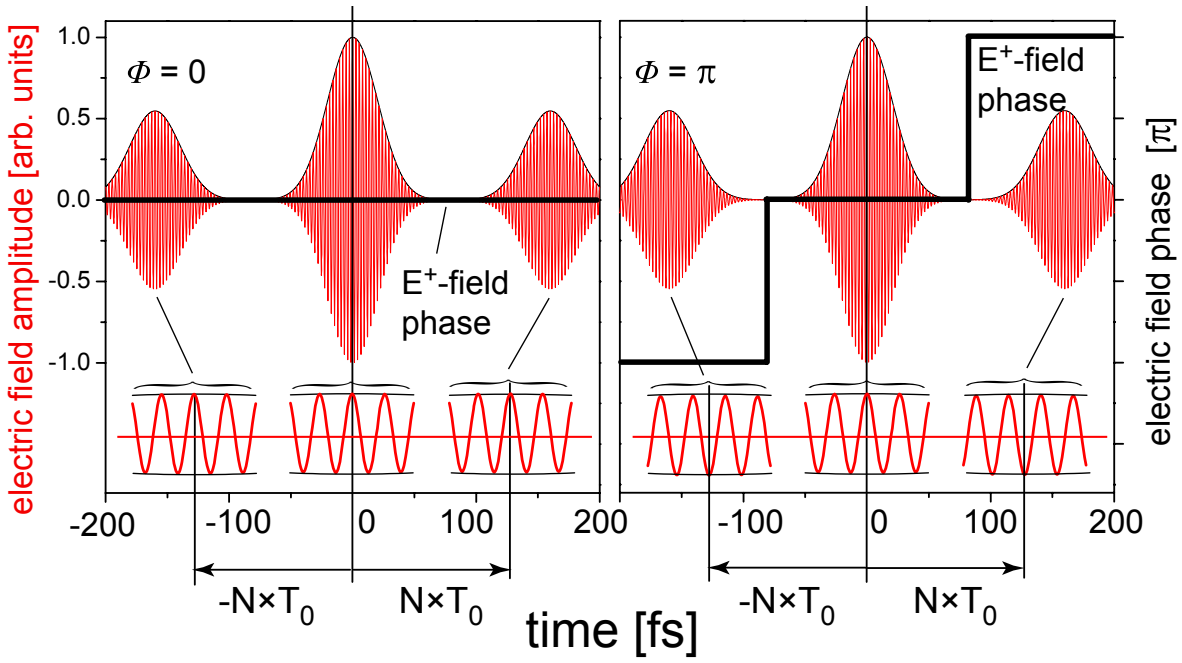

Figure 10.7: Calculated triple pulse sequence in the time domain illustrating the effect of different phase parameters Φ on the pulse sequence. Note that the pulse distance and intensity ratios are not affected by the changing of the parameter Φ. The absolute value of the phase is unknown. Zero phase for the maximum (middle) pulse is assumed.

is utilised without loss of generality because the absolute phase is unknown anyhow and is simultaneously varied as the parameter a is optimised. To mimic the ratio of the side bands of the optimal solution from the free optimisation the parameter $A \simeq 2\pi \times 0.17$ is chosen. In this parameterised optimisation experiment the cleavage of the peptide bond resulting in the fragment with mass $43\,\mathrm{u}$ is again maximised. In this case the convergence is reached after few iterations only. The parametrisation of the phase function speeds up the convergence by an order of magnitude which could be of significant advantage for mass spectroscopic applications. The results lead to a value of the parameter a which corresponds to a pulse separation of $T = 156 \pm 7\,\mathrm{fs}$. This separation is essentially identical to the pulse separation obtained in the free optimisation experiment.

To gain additional information about effects involved in the observed control mechanism, the relative phase of the triple pulses is varied by changing the phase parameter Φ. This change shifts the maximum of the phase modulation function across the LC array. Such procedure has first been introduced in atomic excitation [MSi98] and was recently investigated in great detail for the photoionisation of potassium using photoelectron spectroscopy [WPS06]. The effect

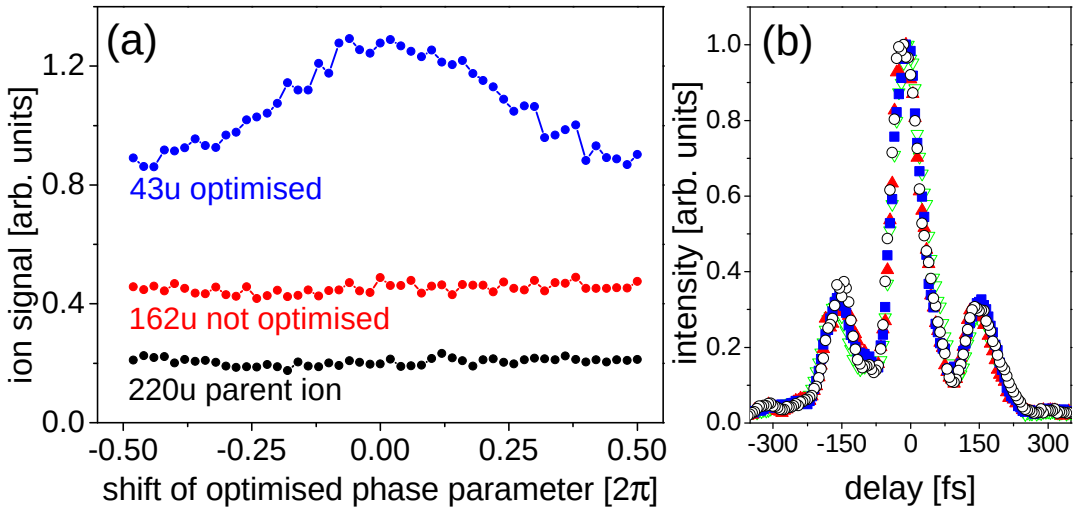

Figure 10.8: (a) Ion yields of mass 43 u, 162 u, and the parent 220 u are plotted as a function of the relative phase shift in the parameterised triple pulses. The signal of mass 43 u varies by about 33% by changing the relative phase. In contrast, the parent ion as well as the suppressed fragment mass 162 u show no distinct relative phase dependence. (b) Measured temporal envelope of the pulse sequence applied for three different relative phase shifts $\Phi = 0, \pi/2$, and $3\pi/2$, illustrating that the pulse shape remains uninfluenced by changing of the relative phase.

of the phase modulation introduces a corresponding shift in the side pulses as is illustrated for two extreme cases $\Phi = 0$ and $\Phi = \pi$, respectively, in Fig. 10.7. The variation of the parameter Φ in a symmetric manner allows one to monitor continuously the fragmentation dynamics as well as the both spectral and phase distribution over the full range of 2π. The absolute phase is not known, and it varies somehow from pulse to pulse without phase stabilisation. However, the relative phase $\Delta\omega T + \Phi$ between the maximum and the side bands can be can be varied from $-\pi$ and π during the experiment.

As clearly visible in Fig. 10.8a the ion yield of fragment mass 43 u depends significantly on the the phase shift among the triple pulses. The phase shift of the optimised triple pulse sequence found by varying only T was arbitrarily defined as zero. Quite remarkably, the yield of parent ions, as well that of the suppressed 162 u fragment exhibits no distinguishable dependence on the phase shift. Projections of recorded SH-XFROG maps onto the time axis corresponding to values of the parameter $\Phi = 0$, $\pi/2$, and $3\pi/2$ demonstrate no measurable

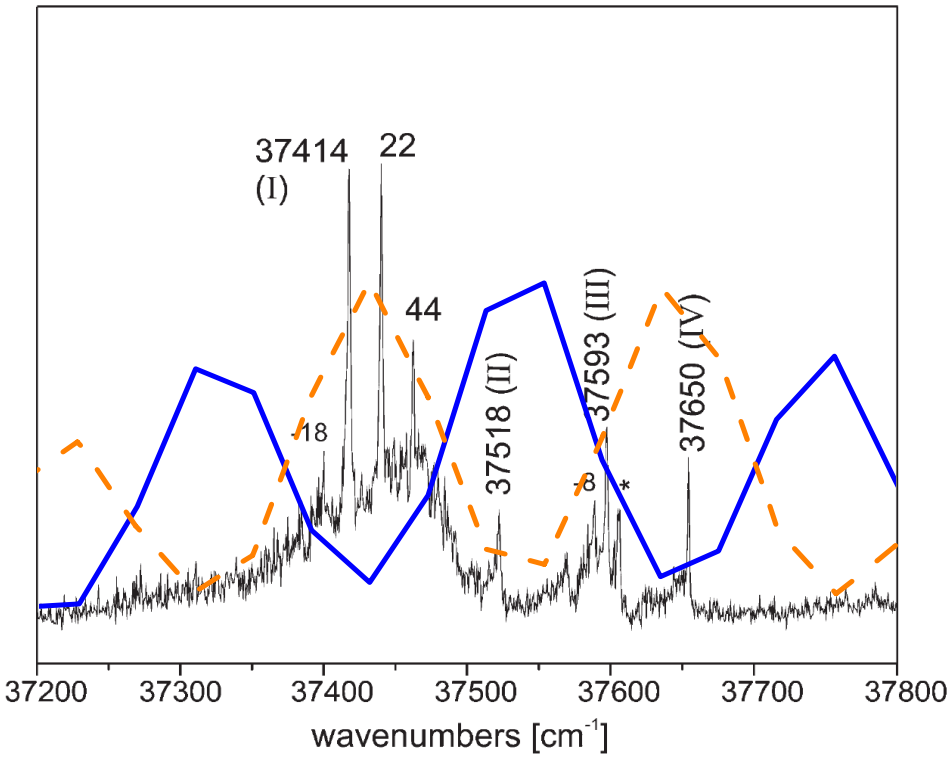

Figure 10.9: Comparison between power spectra of the triple pulses and resonant two photon ionisation spectrum of Ac–Phe–NHMe. The power spectra are calculated assuming a third order process and using phase parameters $\Phi = 0$ and π (blue solid line and orange dashed line, respectively). The resonant two photon ionisation spectrum of Ac–Phe–NHMe in the range of $37200 - 37800\,cm^{-1}$ is taken from [GUG04]. The transitions are labelled with the number of the corresponding isomer (for details see text). The bands at 22 and $44\,cm^{-1}$ belong to isomer I, the bands at -18 and $-8\,cm^{-1}$ are hot bands of isomers I and III, respectively. The band marked by an asterisk arises from a fragment of a AcPheNHMe/water cluster.

effect on the temporal pulse envelope and consequently does not affect its overall intensity as shown in Fig. 10.8b, while the $43\,u$ fragment yield drops by about 33% for $\Phi = \pm\pi$ in comparison to the optimised measurement with phase parameter $\Phi = 0$.

Possibly, the experimentally observed effect of phase sensitivity can be explained considering such effect in the frequency domain, rather than in the time domain and taking into account the spectroscopic properties of the model peptide studied. Fig. 10.9 shows the resonant two photon ionisation spectrum of Ac-Phe-NHMe in the range of $37200 - 37800\,cm^{-1}$ (taken from [GUG04]) together with a pair of power spectra which were calculated by the Fourier transformation of the idealised triple pulses illustrated in Fig. 10.7 and assuming a third order

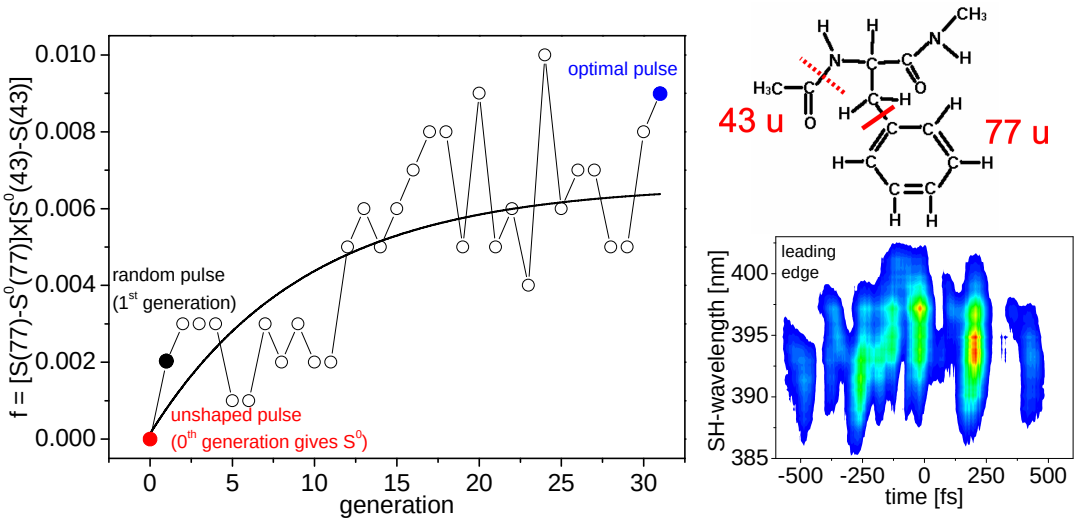

Figure 10.10: SH-XFROG map of the optimal solution and fitness f characterising the enhanced formation of fragment mass 77 u as a function of the generation in the adaptive feedback loop. Large fluctuations of f are due to experimental noise. The solid line is added to guide the eye. On the right, both, the optimised bond cleavage resulting in mass 77 u as a fragment and the suppressed one (43 u) are indicated in the sketch of the Ac–Phe–NHMe molecular structure by the straight and dotted lines, respectively. In addition, SH-XFROG map of the optimal solution is also presented.

process for phase parameters $\Phi = 0$ and π (blue solid line and orange dashed line, respectively). Fig. 10.9 clearly indicates that the variation of the phase parameter Φ leads to the different efficiencies of the laser power absorption by various Ac-Phe-NHMe isomers[1]. Hence, the distinction in Ac-Phe-NHMe fragmentation may be a result of this selective excitation of the isomers.

Fig. 10.10 demonstrates the potential usefulness of the optimal control technique as an analytic tool in mass spectrometry. Here an optimisation run is shown aiming at keeping the peptide bond intact, i.e. the fragment mass 43 u is suppressed in the mass spectra, while splitting the Ac–Phe–NHMe model peptide directly at the benzene ring system. This bond cleavage forms mass 77 u as shown by the sketch in Fig. 10.10. The corresponding learning curve is given as well as the SH-XFROG characterisation of the optimal pulse picked by the algorithm. Although the enhancement is rather limited it is sufficient to obtain a special motif

[1] Isomers are molecules with the same chemical formula, but in which the atoms are arranged differently. They differ in properties because of differences in the arrangement of atoms.

as optimal pulse shape. Small but specific photoinduced changes in the complex fragmentation pattern relative to that of the unshaped pulse may be sufficient to identify chemical constituents in future.

The intensity dependent fragmentation pattern shown in Fig. 10.3 already suggests that strong field effects, such as multielectron excitation of the π-electron ring system and non-adiabatic coupling to nuclear degrees of freedom, are the key for understanding the photophysical and photochemical processes under investigation. Although coherent control and phase sensitivity for atomic systems are now well established and understood, it is by no means evident that the same schemes can explain the high phase sensitivity observed in the present experiment for such a relatively large molecular system. During the strong field and highly non-linear excitation of the presumably neutral molecule with shaped laser pulses selective cleavage of the N1-C3 peptide bond in Ac-Phe-NHMe is increased. This effect may indicate that the critical step in the fragmentation process is the excitation mechanism in the neutral molecules which initiates the propagation of specific wave packets enhanced by the pulse sequence with optimised phases. These wave packets will eventually lead to fragmentation of the system, most probably in the ionic state. It is important, however, that this explanation for the experimental observations at the time being as a very tentative, handwaving interpretation. It is clear that for the elucidation of the detailed molecular reaction dynamics many more experimental evidence is needed and the interplay between experiment and theory will be crucial.

Such further experimental studies will of course involve also different model peptides and in particular different chromophores. As a first step to modify the conditions for energy deposition the chromophore phenylalanine is replaced by alanine while keeping the backbone structure with the protection groups unchanged. Such chemical change is achieved in the model peptide Ac-Ala-NHMe with mass of 144 u.

The aim is to break the same bonds as in Ac-Phe-NHMe. The target chosen for the adaptive control loop is again to maximise the cleavage of the peptide bond (N1-C3) forming the fragment with mass 43 u while keeping the neighbouring bond save, i.e. to suppress the corresponding mass 86 u. The optimal pulse shape as a result of such study is shown in Fig. 10.11. It significantly changes the fragmentation pattern by a factor of 3 and its temporal structure differs very clearly from that found for the Ac–Phe–NHMe model peptide. This again indicates that the photochemical process is presumably driven during the photoexcitation and

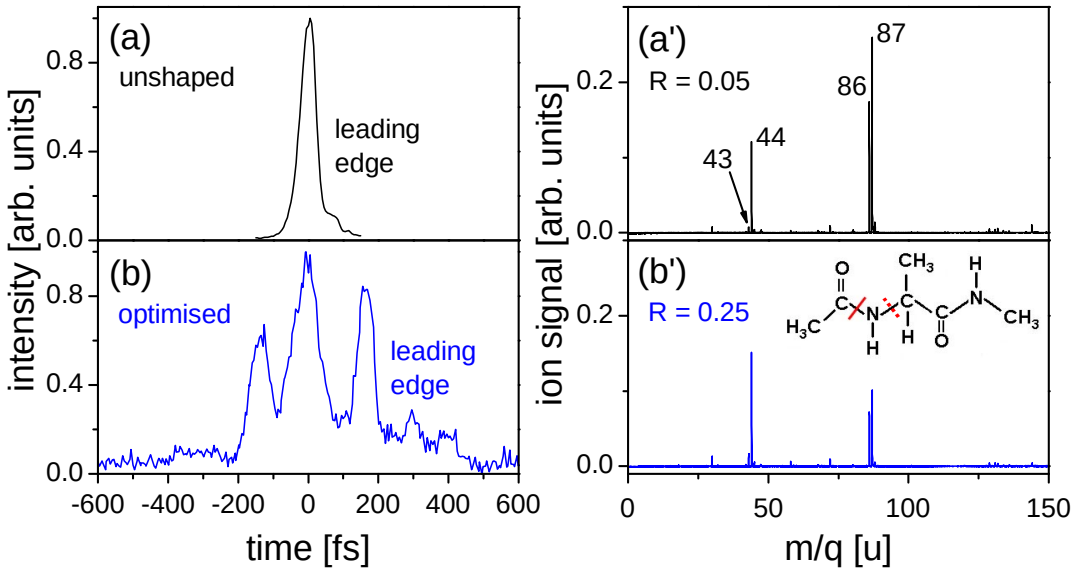

Figure 10.11: Temporal structure (a), (b) and corresponding mass spectra of Ac–Ala–NHMe (a'), (b') are recorded with unshaped and optimal pulse, respectively. The insert shows the molecular structure. Straight and dotted lines indicate the optimised and suppressed bond cleavage, respectively.

not as kind of an afterthought by secondary processes.

Another interesting observation is that the maximum peaks in the mass spectrum do not correspond to the masses expected from a naive look at the chemical structure (43 u and 86 u) which are utilised to define the fitness function as described above. Rather, the protonated species (44 u and 87 u) appear as dominant fragments in the mass spectrum. As one may have expected, the photochemistry of the molecular system sensitively depends on the chromophore even if similar bonds of the backbone structure are taken as target for the adaptive feedback loop. In principle this is good news since mass spectrometry on biomolecular systems with shaped pulses may look for individual pulse forms for individual amino acids. Furthermore, even the dynamics of intramolecular chemical processes, such as proton respectively hydrogen transfer reactions may be investigated by means of optimal control or coherent strategies. This would be another highly relevant application in biophysical research keeping in mind that such type of reactions are assumed to play a key role for the photostability of DNA base pairs [SSR04].